JOURNAL OF GEOPHYSICAL RESEARCH, VOL. 105, NO. B5, PAGES 10,857–10,869, MAY 10, 2000

A crustal model of the ultrahigh-pressure Dabie Shan orogenic belt, China, derived from deep seismic refraction profiling

Chun-Yong Wang and Rong-Sheng Zeng
U.S. Geological Survey, Menlo Park, California
Institute of Geophysics, China Seismological Bureau, Beijing

W. D. Mooney
U.S. Geological Survey, Menlo Park, California

B. R. Hacker
Geological Sciences, University of California, Santa Barbara

Abstract. We present a new crustal cross section through the east-west trending ultrahigh-pressure (UHP) Dabie Shan orogenic belt, east central China, based on a 400-km-long seismic refraction profile. Data from our profile reveal that the cratonal blocks north and south of the orogen are composed of 35-km-thick crust consisting of three layers (upper, middle, and lower crust) with average seismic velocities of 6.0 ± 0.2 km/s, 6.5 ± 0.1 km/s, and 6.8 ± 0.1 km/s. The crust reaches a maximum thickness of 41.5 km beneath the northern margin of the orogen, and thus the present-day root beneath the orogen is only 6.5 km thick. The upper mantle velocity is 8.0 ± 0.1 km/s. Modeling of shear wave data indicate that Poisson's ratio increases from 0.24 ± 0.02 in the upper crust to 0.27 ± 0.03 in the lower crust. This result is consistent with a dominantly felsic upper crustal composition and a mafic lower crustal composition within the amphibolite or granulite metamorphic facies. Our seismic model indicates that eclogite, which is abundant in surface exposures within the orogen, is not a volumetrically significant component in the middle or lower crust. Much of the Triassic structure associated with the formation of the UHP rocks of the Dabie Shan has been obscured by post-Triassic igneous activity, extension and large-offset strike-slip faulting. Nevertheless, we can identify a high-velocity (6.3 km/s) zone in the upper (<5 km depth) crustal core of the orogen which we interpret as a zone of ultrahigh-pressure rocks, a north dipping suture, and an apparent Moho offset that marks a likely active strike-slip fault.

1. Introduction

The Qinling-Dabie Shan orogenic belt was created by the Triassic subduction of the northern edge of the Yangtze craton and subsequent collision with the Sino-Korean craton (Figure 1). Widespread ultrahigh-pressure (UHP) coesite-bearing ecologite facies rocks in the eastern Dabie Shan indicate that during this collision, crustal rocks were subducted to depths >120 km and then exhumed [*Hacker et al*., 1995a]. This Mesozoic orogen, however, is characterized by neither the prominent topography nor thick crust [*Zeng et al*., 1995; *Li and Mooney*, 1998] that is expected in collisional orogens involving subduction of continental crust. To determine the deep crustal structure of the Dabie Shan, a 400-km-long deep seismic refraction profile was recorded in 1994. In this paper we present a two-dimensional (2-D) model of the crustal structure across the Dabie Shan and relate this structure to the processes that created and later modified the orogen. This model supersedes that of *Dong et al*. [1996], who presented a preliminary model based on only a portion of the seismic refraction available data.

Paper number 1999JB900415.
0148-0227/00/1999JB900415$09.00

2. Regional Geologic Setting

The Qinling-Dabie Shan orogenic belt extends WNW-ESE for more than 2000 km and contains abundant high-pressure metamorphic rocks including abundant coesite-bearing eclogite and blueschist facies rocks [*Liou et al*., 1989]. UHP rocks crop out in the three easternmost ranges of the Qinling-Dabie orogen, in the Hong'an, Dabie, and Su-Lu areas (Figure 1). These rocks are believed to have been formed by north directed subduction of the Yangtze craton or of a microcontinent beneath the Sino-Korean craton. Structural [*Hacker et al*., 1995a], metamorphic [*Liou et al*., 1995], and geochronologic [*Hacker and Wang*, 1995; *Hacker et al*., 1998] data from the Dabie Shan have been interpreted to indicate that exhumation of UHP rocks occurred in two stages. In the Triassic-Jurassic, large-scale normal faults brought the UHP rocks from eclogite facies to amphibolite facies depths [*Hacker et al*., 1998]. From 133 to 122 Ma, northwest-southeast extension coincident with voluminous magmatism brought the UHP rocks to within 10–15 km of the surface [*Hacker et al*., 1995a, 1998].

In the Dabie Shan area, there are three east-southeast trending belts separated by faults (Figure 2). (1) The Foziling Group consists of flysch that has been overlain by Cretaceous volcanic rocks. (2) The Dabie Shan contains a prograde high- to ultrahigh-pressure metamorphic sequence in its southern

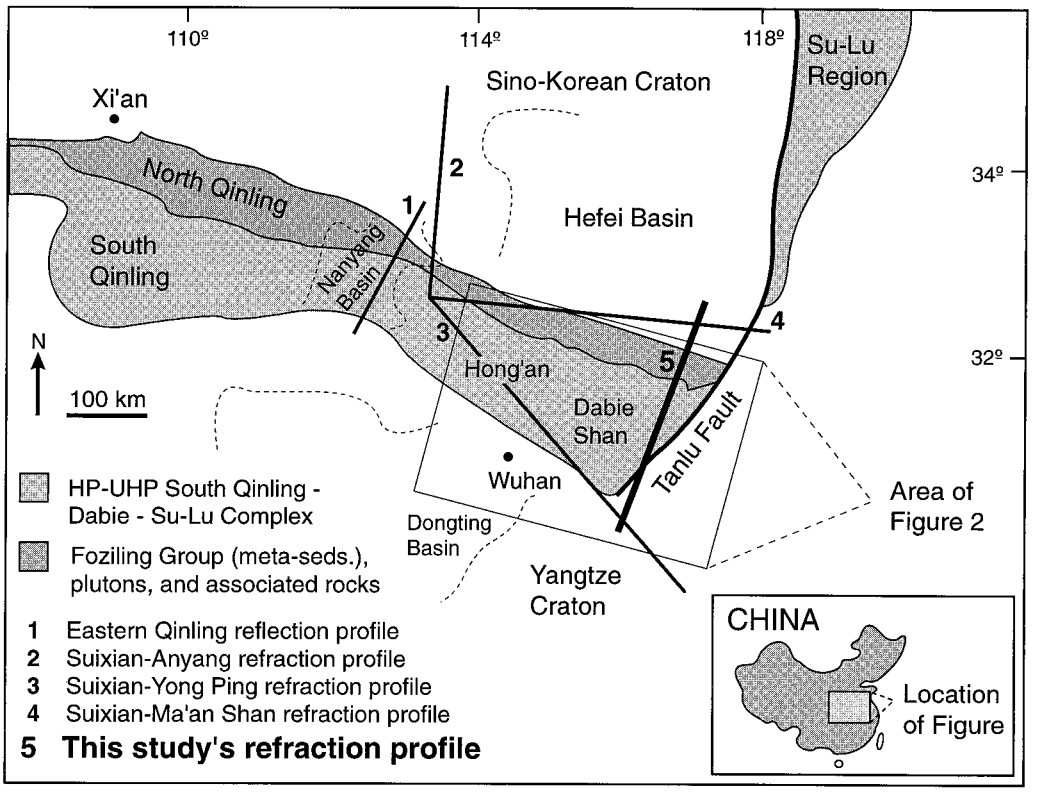

Figure 1. Geologic map of the Qinling-Dabie Shan orogenic belt in the central eastern China. The region is exceptional for the widespread occurrence of ultrahigh-pressure rocks, including coesite-bearing eclogite and rare diamonds. The Su-Lu region is displaced to the northeast of Dabie Shan by the Tan-Lu fault. Previously published seismic reflection and refraction profiles are indicated (citations in text).

half and Cretaceous plutons and orthogneiss in its northern half [*Hacker et al*., 1995a]. (3) The Foreland fold belt comprises a thick series of late Proterozoic felsic volcanic rocks and fine-grained sedimentary rocks overlain by Late Proterozoic to Middle Triassic sandstone, limestone, and shale. South of the Foreland fold belt, there are east-west trending folds with several kilometer long wavelengths that continue across the southward projection of the Tan-Lu fault.

The Dabie Shan complex and the Foziling Group are abruptly truncated to the east by the Tan-Lu fault (Figures 1 and 2). This apparently sinistral fault may have formed in the Triassic during the continental collision between the Sino-Korean and Yangtze cratons [e.g., *Yin and Nie*, 1993], and dextral displacement is thought to have continued through the Jurassic and Early Cretaceous [*Xu et al*., 1987; *Chen et al*., 1988]. Today this fault is expressed as a post-Late Cretaceous normal fault between the Dabie Shan complex and the Foreland fold belt.

3. Previous Geophysical Results

Although this study is the first seismic profile across the Dabie Shan itself, there are several nearby seismic reflection and refraction profiles (Figure 1). The Eastern Qinling reflection profile [*Yuan et al*., 1994] is ~300 km west of the Dabie Shan. This profile images the Qinling orogen that separates the Sino-Korean and Yangtze cratons. According to *Yuan et al*. [1994] the reflection data provide evidence that late in the collision process the lower crust of the Qinling orogen was subducted southward beneath the Yangtze craton, whereas the upper crust, was overthrust on a large scale to the south.

Three seismic refraction profiles are located west, south, and north of the orogen (Figure 1). These are the Suixian-Anyang profile [*Hu et al*., 1986], the Suixian-Yongping profile [*Group of Industrial Explosion Observation*, 1988] for which a geoscience transect was compiled [*Wang et al*., 1995], and the Suixian-Ma'an Shan profile [*Zheng and Teng*, 1989]. All three profiles recorded industrial explosions near the city of Suixian. South of the Dabie Shan, the crustal thickness is 34 km, and the average crustal velocity is 6.35 km/s [*Group of Industrial Explosion Observation*, 1988]. North of the Dabie Shan, the Hefei basin has a 32-km-thick crust with an average velocity of 6.25 km/s [*Zheng and Teng*, 1989]. The Suixian-Anyang profile passes through the southern portion of the Sino-Korean cra-

Table 1. Locations of Shot Points

Shot Point	Name	Latitude N	Longitude E
ZhM	Zhuangmu	32°23.6′	117°07.7′
GuT	Guantin	31°50.1′	116°52.3′
BuT	Butasi	31°28.9′	116°44.5′
ZhZ	Zhuangzhong	30°43.3′	116°17.2′
JnG	Jinggong	30°46.6′	116°52.3′
ErL	Erlanghe	30°15.3′	116°03.1′
CaS	Caishan	29°51.6′	115°48.9′
ZhG	Zhuanggongdu	29°09.1′	115°39.1′

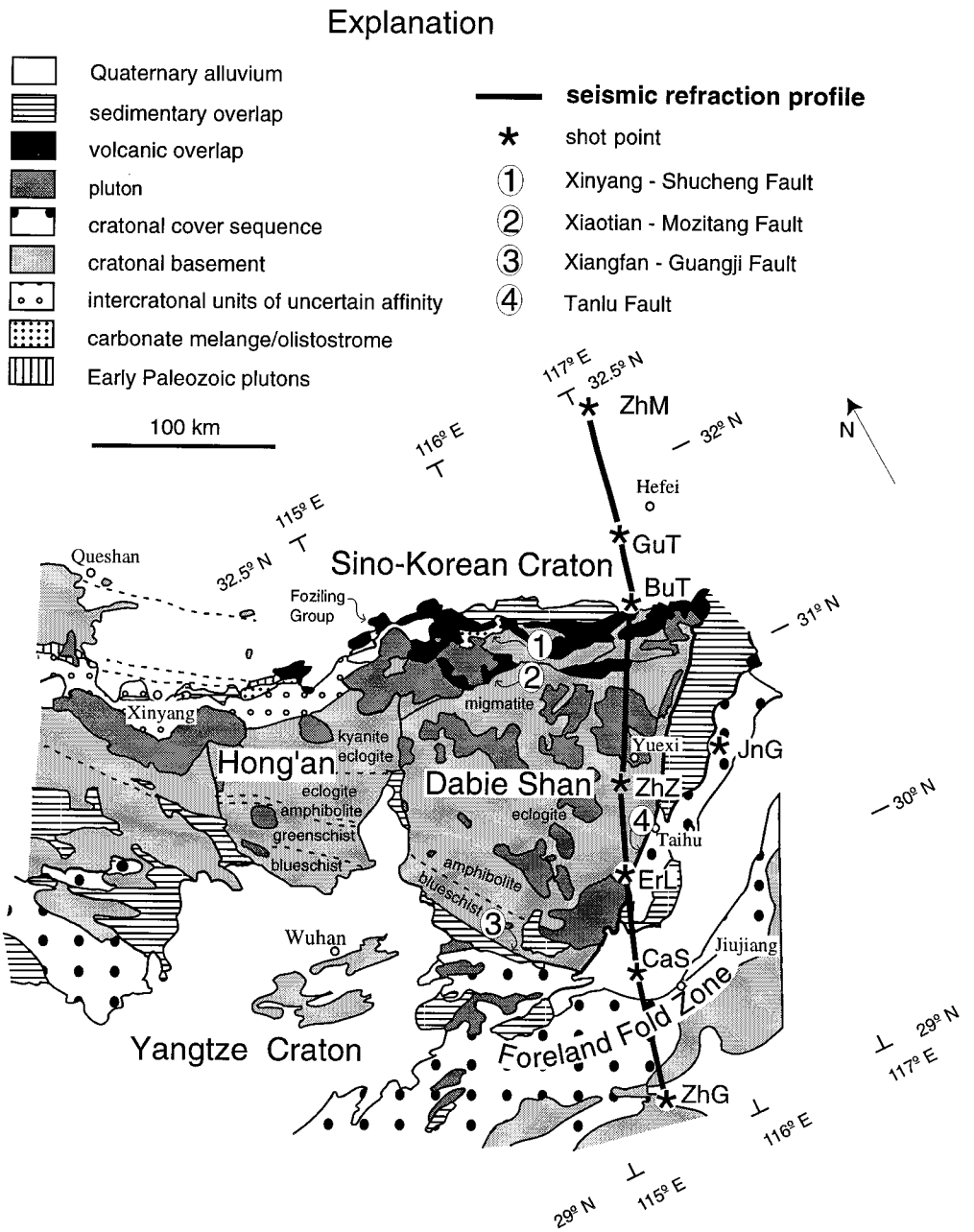

Figure 2. Geologic setting of the Dabie Shan and location of the seismic refraction profile [after *Hacker et al*. [1995b]. Shot points are ZhM (Zhuangmu), GuT (Guantin), BuT (Butasi), ZhZ (Zhuangzhong), JnG (Jinggong), ErL (Erlanghe), CaS (Caishan), and ZhG (Zhanggongdu).

ton, which has a 34-km-thick crust with an average velocity of 6.30 km/s [*Hu et al*., 1986].

The Bouguer gravity data in the study area delineate an ellipsoidal negative anomaly with a −50 mGal average and −75 mGal low centered on the Dabie Shan (i.e., 50 km west of shot point ZhZ, Figure 1) [*Qiu and Guo*, 1989]. The negative anomaly correlates with higher topography (~1200 m) and a small (6.5 km) crustal root, as described below. The gravity data have not been modeled in this study.

4. Layout of the Profile

Our seismic refraction profile trends N25°E and begins in the north within the Hefei basin of the Sino-Korean craton, passes through the Dabie Shan, and ends in the Yangtze craton. The profile crosses four significant strike-slip faults from north to south: the Xinyang-Shucheng, Xiaotian-Mozitang, Xiangfan-Guangji, and Tan-Lu faults (Figure 2).

Eight shots (Table 1) were recorded by a total of 150 analog recorders. Seismic energy was generated by borehole explosions, with the exception of the shot at ZhZ (Figure 2), which was an underwater explosion. Shotpoints were spaced ~50 km apart, with the exception of shot points BuT and ZhZ which were ~90 km apart. The explosive charge of each shot varied from 1000 to 2000 kg, based on the site conditions and the maximum shot-recorder distance. Seismic recorders were spaced 3–4 km outside the orogen and were 1 km apart within the orogen to obtain higher resolution. Most recorders were

three-component seismographs with 1-Hz geophones. The analog records were digitized with a 10-ms sampling interval.

5. Data Interpretation

5.1. General Analysis of Seismic Phases

A complete set of all record sections are presented here. Details of the individual sections will be discussed below. Methods of interpretation of seismic refraction data and model uncertainties are discussed by *Mooney* [1989], who estimates that seismic velocities are accurate to better than 3% and boundary depths (e.g., Moho) are accurate to better than 10% of the calculated depth. The phases Pg and Pn are recognizable as the first arrivals on all record sections. Pg, the refracted wave propagating within the upper crust, is observed at distances of $<$100 km. Pn, the refraction within the uppermost mantle, is a first arrival at distances beyond 160 km.

Besides the Pg and Pn phases, four other phases can be recognized as secondary arrivals with highly variable clarity. The most prominent secondary phase, PmP, is a wide-angle reflection from the crust-mantle boundary. This phase is visible for all shots. Additional wide-angle reflections, labeled P_1, P_2, and P_3, are variably observed from intracrustal interfaces. These reflections are generally weaker than PmP. One reason for this may be seismic scattering caused by fine-scale structure [*Levander et al*., 1994]. While it is generally accepted that the crust is grossly layered and that velocity generally increases with depth [*Meissner*, 1986; *Mooney and Brocher*, 1987; *Christensen and Mooney*, 1995], fine-scale structure can also effect the seismic response of the crust. Numerical modeling demonstrated that such fine-scale structure can be misinterpreted to indicate crustal layering [*Mereu and Ojo*, 1981; *Ojo and Mereu*, 1986; *Levander and Holliger*, 1992; *Levander et al*., 1994]. Our interpretation is based on the assumption that the phases P_1, P_2, and P_3 are ray geometric (i.e., specular) reflections. However, we acknowledge that fine-scale structure probably is also significant. It is unlikely, based on the evidence from global seismic reflection profiles, that the crust contains continuous, smooth specular reflectors at the scale of this study [*Levander and Holliger*, 1992]. Thus our model is an internally consistent (i.e., satisfying observations from multiple sources and receivers), layered approximation to a heterogeneous crust. Only significantly more dense seismic data will reveal how close this model is to the fine-scale structure.

5.2. Shot Point ZhM (Zhuangmu)

Shot point ZhM (Figure 3) is located in the Hefei basin of the Sino-Korean craton. Pg has an apparent velocity of 6.15–6.25 km/s at distances from 40 to 75 km. P_1 is a reflection with an apparent velocity of 6.2 km/s between 55 and 90 km. Reflection P_2 is observed between 100 and 140 km with an apparent velocity of 6.2–6.3 km/s. However, the precritical reflection for the phase P_2 is not clear at distances of $<$100 km, perhaps due to crustal scattering, as mentioned above. PmP is a very clear, high-amplitude phase from 70 to 270 km. The PmP waveform near the critical angle is remarkably simple, with an abrupt onset that we have modeled using synthetic seismograms with a first-order transition and a significant ($\sim$1.0 km/s) jump in velocity. Such crisp PmP waveforms are common in regions that have experienced crustal extension, such as much of western Europe and the Basin and Range [*Catchings and Mooney*, 1991; *Jarchow et al*., 1993]. The average crustal velocity, calculated from PmP travel times between 70 and 200 km on the section ZhM, is 6.25 km/s. A strong secondary phase with a low apparent velocity of $\sim$6.1 km/s that appears to be a continuation of PmP is observed from 200 to 270 km following Pn. This phase (P_x) cannot simply be the asympotic wide-angle PmP reflection because, in this case, the apparent velocity would be equal to the velocity of the lower crust (6.6–6.9 km/s in this region). The travel time and amplitude of this phase are similar to a prominent phase observed on the Suixian-Ma'an Shan profile [*Zheng and Teng*, 1989] are several possible interpretations of it. *Zheng and Teng* [1989] considered it to be a diffracted wave from the Moho. However, we are able to obtain an excellent travel time fit to the phase P_x with a reflection from the bottom of a modest low-velocity zone at a depth of 17 km. This interpretation is essentially the same as that of *Ye et al*. [1995], who observed a similar prominent phase in data from the Swiss Alps. Pn is a clear first arrival beyond the distance of 160 km and has an apparent velocity of about 8.0 km/s.

5.3. Shot Point GuT (Guantin)

Shotpoint GuT (Figure 3) is also in the Hefei basin, $\sim$66 km south of shot point ZhM. In record section GuT-north the apparent velocity of Pg is about 6.15 km/s, in agreement with the reversing data from shot point ZhM. On section GuT-south the apparent velocity of the Pg phase is 6.2 km/s. Phase P_1 has an apparent velocity of 6.25 km/s between 70 and 110 km. P_2 is a clear reflection at distance between 120 and 160 km, but is very weak at pre-critical distances. PmP is the highest amplitude arrival at distance between 80 and 140 km, but it is not clear beyond 140 km. Pn, with an apparent velocity of 8.1 km/s, is observed as a clear first arrival beyond 170 km.

5.4. Shot Point BuT (Butasi)

Shot point BuT (Figure 4) is located in the Foziling schist, $\sim$10 km north of the active strike-slip Xinyang-Shucheng fault, and $\sim$40 km north of the Cretaceous left-lateral, normal Xiaotian-Mozitang fault. On section BuT-north the apparent velocity of Pg is 6.0 km/s, 0.2 km/s less than the reversed observation (section GuT-south). A deepening of the basement to the north is likely to cause this difference. The phase P_1 can be traced between 30 and 70 km. The phases P_2 and P_3 cannot be recognized on the north section due to the sparse station spacing. PmP is clearly observed at distances of 70–110 km.

On record section BuT-south, Pg arrival times are about 0.5 s earlier than on the section to the north. This confirms a northward dipping basement. In addition to P_1, there are two intracrustal reflection phases (P_2 and P_3) that are variably visible on the section. Phase PmP is once again very clear and is dominant at distances between 90 and 160 km. PmP travel times at distances of 90–140 km on record section BuT-south are $\sim$1.0 s later than the travel time on section BuT-north. This indicates that the Moho deepens to the south of BuT. The PmP travel times for BuT-south are also about 1.0 s later than for GuT-south (Figure 3), also indicating that the Moho deepens south of shot point BuT.

5.5. Shot Point ZhZ (Zhuangzhong)

Shot point ZhZ (Figure 4) is located within the coesite-bearing eclogite unit, with the receivers to the south passing through the UHP zone. The Cretaceous synmagmatic normal fault that dropped the coesite-eclogite unit down relative to the northern orthogneiss in the footwall is exposed a few kilometers north of the shot point. Unlike the other shots, the explo-

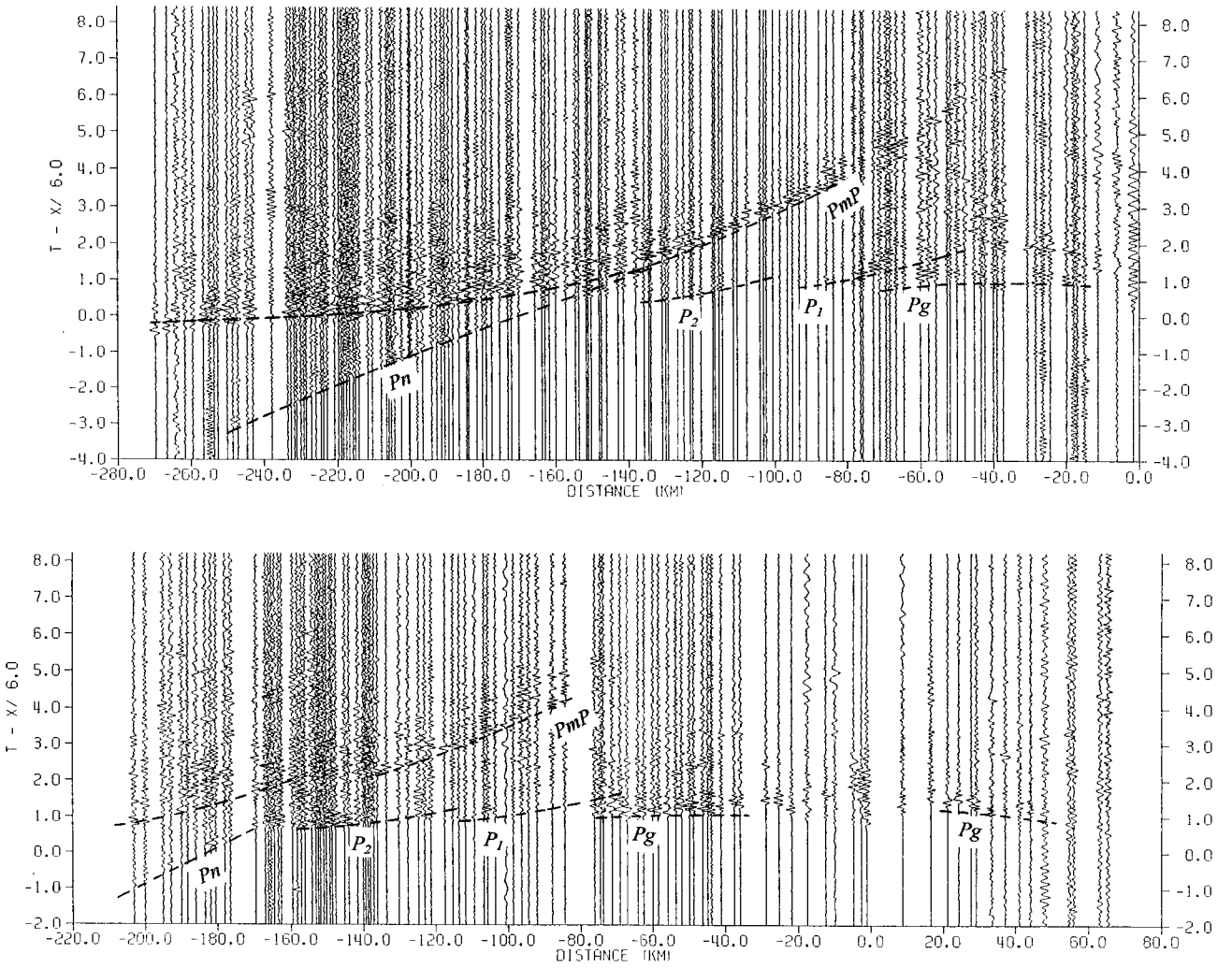

Figure 3. (top) Trace-normalized low-pass filter (10 Hz) record section of shot point ZhM. For this and all other record section the travel time curves are theoretical curves calculated from the final velocity model. Shot point locations are shown in Figure 2. The dominant phases on the section are (1) *PmP* (reflection from Moho), which has a very simple waveform near the critical distance (~120 km), and (2) P_x, which has a low (6.1 km/s) apparent velocity and is interpreted as a wide-angle reflection from the bottom of midcrustal low-velocity zone (see text for additional discussion). The phase refracted just below the Moho (*Pn*) is clearly recorded as a first arrival. The corresponding shear wave phase *Sn* was not observed. (bottom) Record section of shot point GuT. The dominant phase *PmP* stops at about 145 km. The intracrustal phases P_1 and P_2 are weakly recorded at precritical distances (less than ~80 km), possibly due to scattering in the crust.

sion was detonated under water, and reverberations with higher-frequency content are observed on the records.

On record section ZhZ-north, *Pg* has an apparent velocity of 6.0 km/s. The upper crustal reflection P_1 is weaker than that in the section to the south. Phase P_2 can be traced from 50 to 120 km. P_3 is not at all clear. *PmP* is the strongest phase on the section beyond 80 km.

On record section ZhZ-south, *Pg* has an apparent velocity of 5.95 km/s. A distinct phase P_1 with larger amplitude than that of the *Pg* phase can be traced from 20 to 70 km. This phase is also strong on the section JnG-south (see below). The phases P_2 and P_3 are not clearly observed. The shot point-recorder distances are too short to record either *PmP* or *Pn*.

5.6. Shot Point JnG (Jinggong)

Shot point JnG (Figure 5) is located on the Yangtze craton, east of the Tan-Lu fault. It is offset ~50 km east of the main line. Because the main line is not perfectly straight, the records beyond 70 km can be approximated as in-line observations (Figure 2). The travel time of the phase *PmP* for propagation to the north is similar to ZhZ-north. The phase *PmP* is also clearly observed on section JnG-south, and this observation is important in view of the lack of *PmP* from section ZhZ-south.

5.7. Shot Point ErL (Erlanghe)

Shot point ErL (Figure 5) is located in the southern half of the high-pressure metamorphic belt, just west of the Tan-Lu fault. The apparent velocity of *Pg* is 5.95 km/s, in agreement with section ZhZ-south. Although the phase P_1 behind *Pg* can be traced to 120 km, its energy is weaker than the P_1 on section ZhZ-south. Similar to section BuT-south, phase P_2 is strongest at distances of 120–150 km. *PmP* is dominant beyond 80 km and consists of a simple waveform with an abrupt onset. The arrival time at 100 km is 0.5 s earlier than on sections ZhZ-

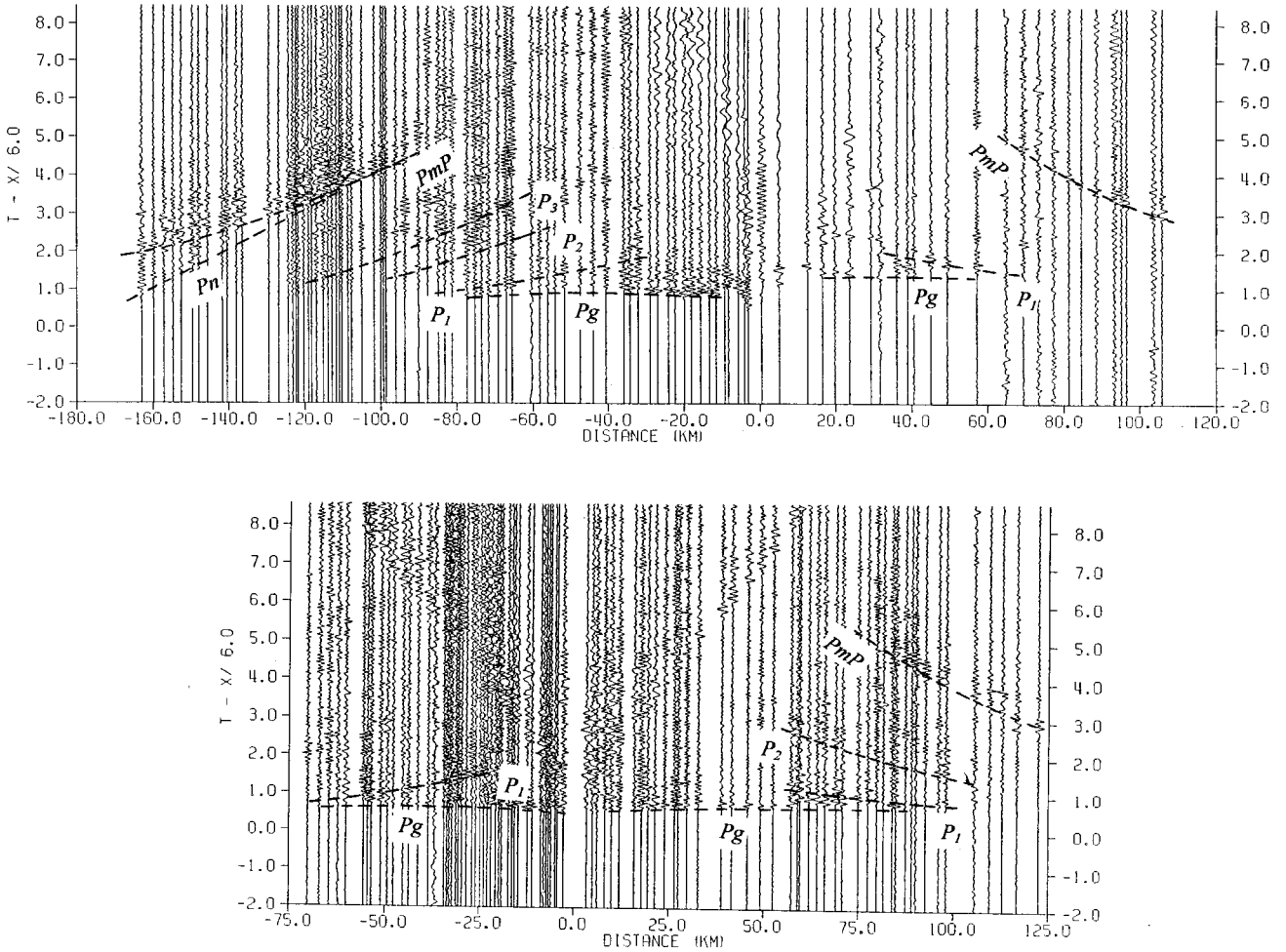

Figure 4. (top) Trace-normalized low-pass filter (10 Hz) record section of shot point BuT. The Moho reflection, PmP, is a strong phase in the data recorded to the south. Two intracrustal reflection phases, P_2 and P_3, are evident with variable amplitude before the phase PmP. Station spacing averaged 4 km to the north of the shot point. (bottom) Record section of shot point ZhZ. A distinct reflection phase (P_1) is evident 0.3 to 0.7 s behind the Pg phase on the record section to the south. The Moho reflection, PmP, is clearly recorded to the north, and there is abundant seismic energy following the first arrival, Pg, and before PmP. We identify three intracrustal reflected phases, P_1, P_2, and P_3, but scattering may also contribute to this seismic energy.

north and BuT-south. Pn is weaker than on sections of ZhM and GuT-south. Except for Pg and PmP, all of the phases on the section are weaker than on the section BuT-south.

5.8. Shot Point CaS (Caishan)

Shot point CaS (Figure 6) is located in the fold-thrust belt south of the Dabie Shan, close to the Yangtze River. On section CaS-north, Pg is generally obscured near the shot point due to the high background noise. P_1 and P_2 are observed variably. The arrival time of PmP is basically the same as that of ErL-north. The profile is not long enough for Pn to be recognized as the first arrival. Although there is only a short observation distance (~10 km) south of the shot point, we can easily see from the late Pg arrival time that the basement deepens beneath the Yangtze River valley.

5.9. Shot Point ZhG (Zhanggongdu)

Shot point ZhG (Figure 6) is located in the Yangtze craton. Pg can be traced from 10 to 60 km with an apparent velocity of 5.9 km/s. Between Pg and PmP, intracrustal reflection P_2 is evident from 70 to 110 km. The PmP travel time at a distance of 100 km is similar to that on sections CaS and ZhM. Pn appears beyond ~160 km as the first arrival and has an apparent velocity of ~7.9 km/s.

6. Two-Dimensional Modeling

A finite difference tomographic inversion method [*Vidale*, 1988, 1990] was used to model the upper crustal velocity structure based on the Pg arrivals. Modeling of the middle and lower crust and uppermost mantle was then carried out using 2-D forward ray tracing. The travel times and amplitudes of all of these seismic phases have been calculated using the programs "MacRay" [*Luetgert*, 1992] and "SEIS-83" [*Cerveny et al.*, 1977; *Cerveny and Psencik*, 1984]. Synthetic seismograms have been calculated using the asymptotic ray theory [*Cerveny and Psencik*, 1984].

In the finite difference travel time method, travel times are extrapolated outward from the source region to each point in the model [*Vidale*, 1988, 1990]. We used an inversion method

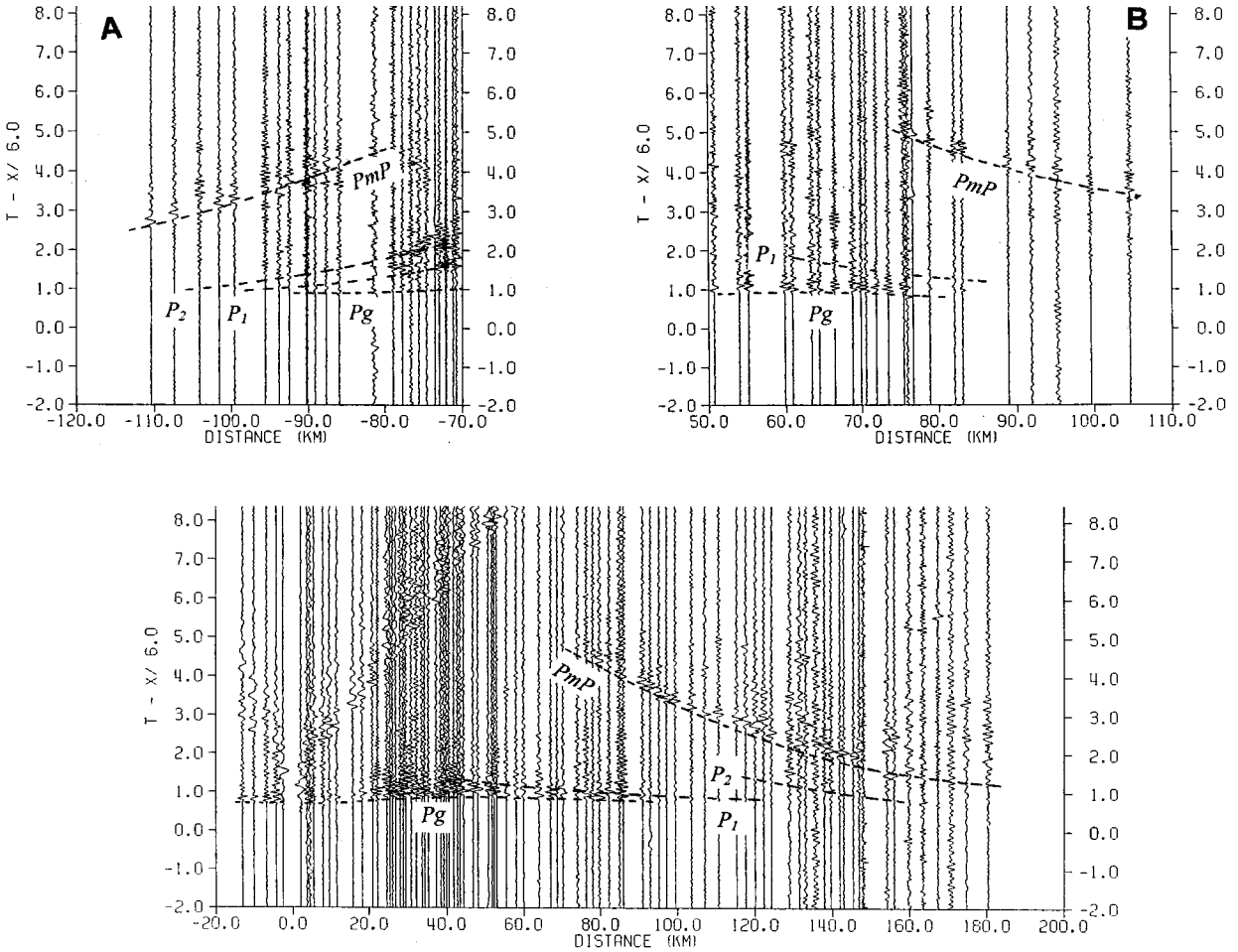

Figure 5. (top) Trace-normalized low-pass filter (10 Hz) record section of shot point JnG, which was located off-line. The reflection from Moho, PmP, is clearly recorded and is delayed on the section to the north relative to the section to the south. Intracrustal reflections, labeled P_1 and P_2, are clear only on the data to south where the station spacing is 1–2 km (70–80 km distance range). (bottom) Record section of shot point ErL. The PmP reflection is very clear, and the travel time curvature constrains the average crustal velocity to ~6.3 km/s. The intracrustal reflection P_2 is well recorded at distances around 140 km. The refraction from to uppermost mantle, Pn, is not visible in these data.

capable of imaging media containing strong velocity variations [*Ammon and Vidale*, 1993; *Hole*, 1992]. The inversion model was parameterized using 4-km cells. To maintain accuracy, a uniform 1 km square grid was used for the travel time calculation. A total of 479 Pg arrival times were used in the inversion. The final velocity model (Figure 7a) was obtained after 5 iterations. The RMS travel time residual decreased from 0.35 to 0.10 s for the model. There is no significant difference between the models obtained after 5 and 10 iterations. The resolution of the inversion was assessed by summing the number of rays traveling through each cell (Figure 7b). The central part of the profile (between 90 and 270 km) was covered by more than 25 rays. The rays in the area between 100 and 200 km on Figure 7b do not penetrate below a depth of ~5 km due to the presence of a high-velocity zone. Velocities at depths <5 km are well resolved, especially in the central part of the profile. The most prominent feature is a high-velocity (6.3 km/s) zone beneath shotpoint ZhZ, in the middle of the UHP zone. We discuss this feature below.

The crustal structure below ~10 km was determined from the wide-angle reflections. As discussed earlier, phase P_1 has a high amplitude on the record section of ZhZ-south. The difference of travel time between P_1 and Pg at distances of 20 and 70 km are 0.75 and 0.3 s, respectively. The calculation of synthetic seismograms indicates that a higher velocity layer (6.4 km/s) beneath an interface at a depth of ~7 km provides a good match to the Pg/P_1 amplitude ratio. The high-velocity (6.4 km/s) layer is modeled as a thin layer in order to fit the travel times of later arriving phase, (i.e., P_2, P_3, PmP) and because a thicker layer at shallow depth would cause an unreasonably large gravity anomaly.

Figure 8 shows the comparison between observed and calculated travel time data and between observed and synthetic seismograms from shot point BuT. The observed and calculated travel times and amplitudes are in reasonable agreement. The greater complexity of the observed wave field compared with the synthetic wave field indicates that the crust does not contain continuous, smooth specular reflectors, as was mentioned earlier. Scattering in the crust may also contribute to the amplitude misfits between the calculated and observed intracrustal phases.

The 2-D crustal velocity structure across the Dabie Shan is shown in Figure 9a. The contoured velocity values are the

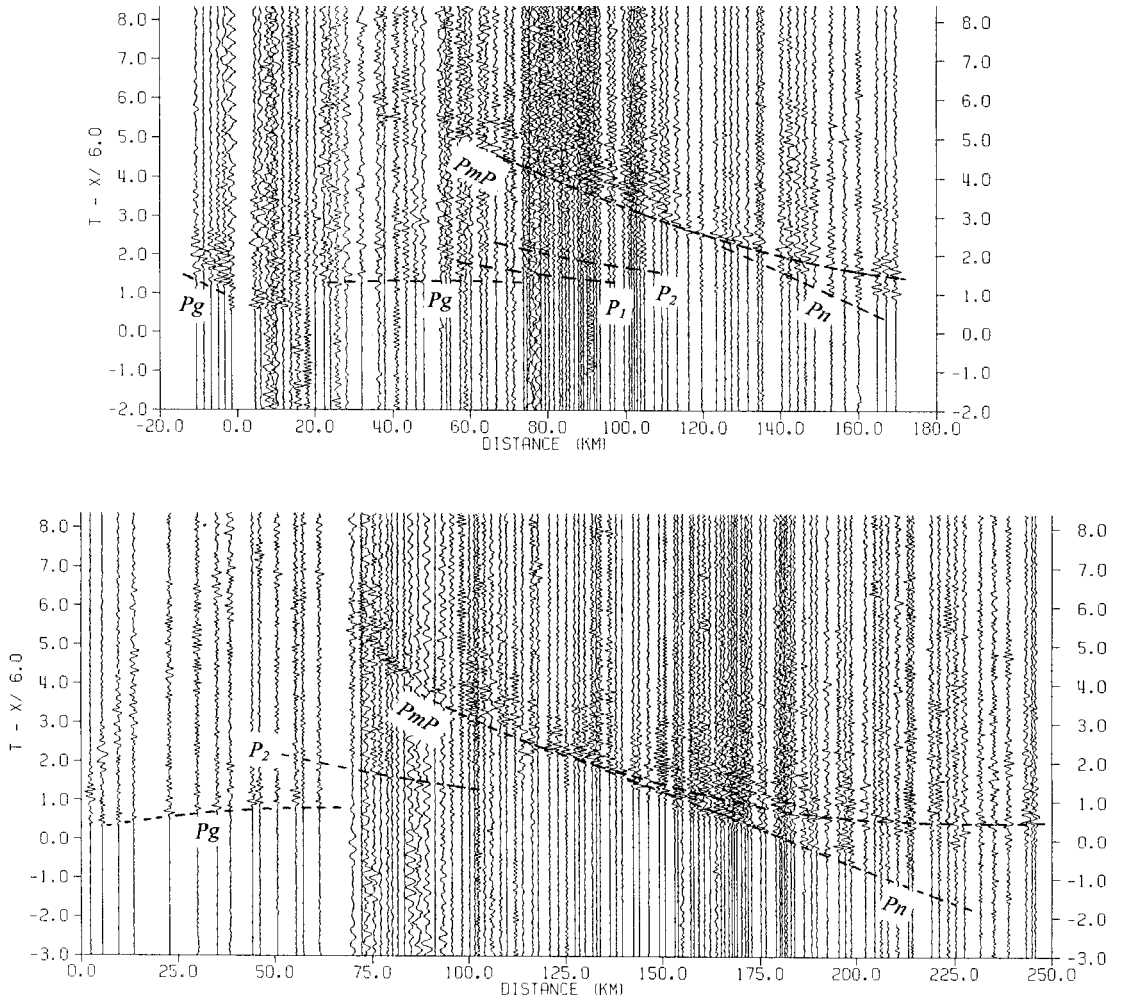

Figure 6. (top) Trace-normalized low-pass filter (10 Hz) record section of shot point CaS. *PmP* is clearly observed, but the intracrustal reflections P_1 and P_2 are not highly coherent phases, even in the most densely recorded portions of the profile. Seismic scattering may play a role in the generation of the P_1 and P_2 phases. (bottom) Record section of shot point ZhG. *PmP* and *Pn* arrival phases are clearly observed. These observations, together with the reversing profile from shotpoint ZhM-south, and provide strong constraints on the average crustal velocity, crustal thickness and uppermost mantle velocity.

result of interative forward modeling of seismic travel times of phases arriving after *Pg*. The location of seismic control on the depth of the crustal boundaries is indicated by heavy solid lines. The Moho discontinuity is ~6 km deeper beneath the Xiaotian fault than beneath the Sino-Korean and Yangtze cratons, where an offset of ~3.5 km appears to exist. The Moho offset was inferred from (1) a travel time difference of 1.0 s for the *PmP* reflection as recorded from shot points GuT and BuT, even though the distance between the two shot points is only 40 km (Figures 3 and 4); (2) *PmP* arrivals from shot point GuT-south, which are very clear from 90 to 145 km and are abruptly interrupted at the distance of ~145 km (Figure 3); and (3) the clear travel time difference of 1.0 s for *PmP* from BuT-north versus BuT-south (Figure 4).

7. *S* Wave Velocity and Poisson's Ratio

The horizontal components of the seismic records were used to determine the shear wave velocity structure beneath the Dabie Shan. The phases *Sg* and *SmS* appear clearly on the record sections of most shot points (e.g., ErL in Figure 10). However, the uppermost mantle phase *Sn* can not be identified on the record sections. In addition, the converted wave *PmS* reflected from the Moho can be recognized on the records of BuT and JnG. The *S* wave velocity model was obtained using two-dimensional ray tracing, as for the *P* wave model. *S* wave velocities and Poisson's ratio within the crust are shown in Figure 9b. Fourteen out of fifteen values of Poisson's ratio are in the range 0.23–0.27 (one value is 0.29). Because the *S* wave phases reflected on the intracrustal interfaces are generally more difficult to identify than *P* wave reflections, the *S* wave velocities in the midcrust have larger uncertainties. However, the very clear *PmP* and *SmS* reflections provide very good constraints on the average whole crustal Poisson's ratio (0.25–0.26; Figure 9b). The fact that the many record sections contain both clear *Pn* and *SmS* phases, but lack the phase *Sn*, may indicate a negative *S* wave velocity gradient in the uppermost mantle.

Our seismic model indicates that Poisson's ratio, which is an indicator of crustal composition [e.g., *Holbrook et al.*, 1992; *Christensen*, 1996] varies with depth from 0.23–0.26 in the

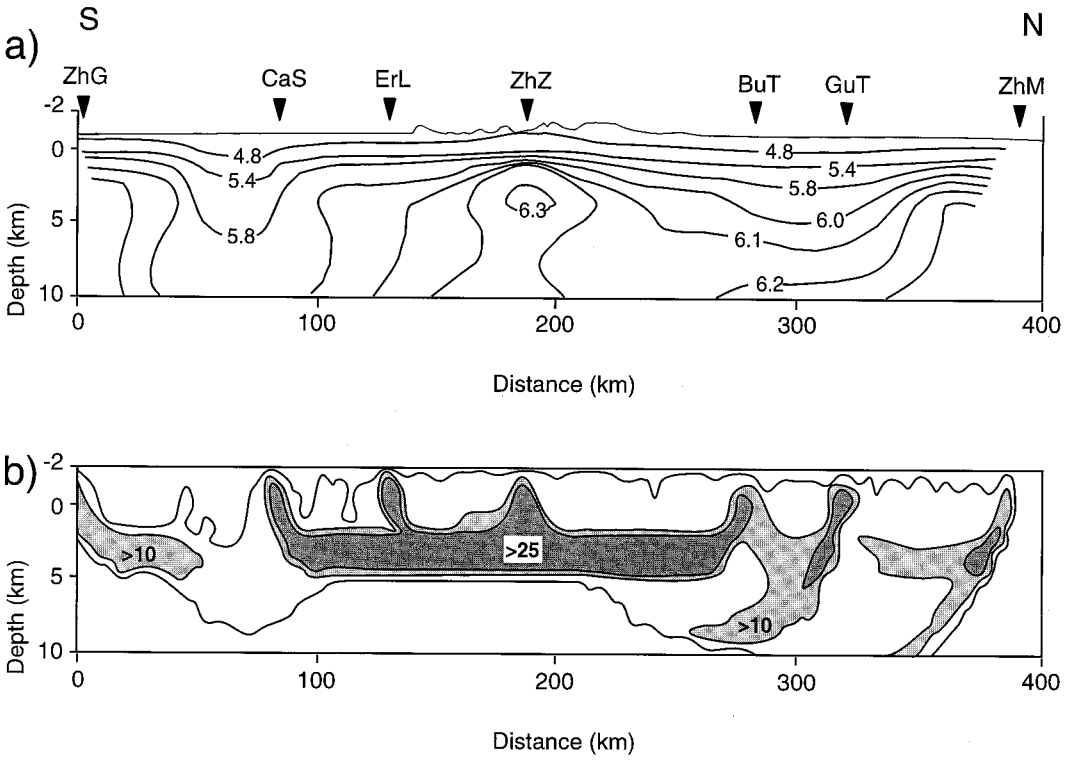

Figure 7. Upper crustal velocity structure (a) Model with velocity isolines (km/s) derived from finite difference travel time inversion. The high-velocity zone (6.3 km/s) correlates with the antiformal core of the uppermost crust of the orogen where ultrahigh-pressure rocks occur. (b) Number of rays traveling through each cell. The central part of the profile (between 80 and 280 km) was covered by sufficient rays and the inverted velocities at depths are reliable. The rays in the interval between 100 and 200 km do not penetrate below the depth of ~5 km due to the high velocity zone (6.3 km/s).

upper crust to 0.26–0.29 in the lower crust. Estimated uncertainties are 0.02–0.03. The composition of the crust of eastern China, including the area of the Dabie Shan orogen, has previously been discussed by *Gao et al.* [1998], *Li and Mooney* [1998], and *Kern et al.* [1998]. The combined compressional and shear wave model (Figure 9) is consistent with these previous models for an upper crustal composition of felsic metasedimentary and granitic rocks, a middle crust of intermediate (dioritic) composition, and a lower crustal composition of intermediate-to-mafic rocks in the amphibolite to granulite metamorphic facies. There is no seismic evidence for a volumetrically significant amount of high-velocity eclogite within the deeper crust, despite the fact that eclogite is locally exposed within the Dabie Shan [*Kern et al.*, 1998].

8. Discussion

Despite significant collisional convergence in the Mesozoic and the presence of surficial ultrahigh-pressure rocks, only a modest crustal root presently exists beneath the Dabie Shan. The crust thickens from 35 km beneath the Yangtze craton to 41.5 km at the northern margin of the Dabie Shan and thins to 34 km beneath the Sino-Korean craton. The average velocities of the crust beneath the Yangtze craton, the Dabie Shan, and the Sino-Korean craton are 6.35, 6.30, and 6.25 km/s, respectively. Both the Yangtze craton and the Sino-Korean craton have a three-layer crustal structure with velocities of 6.0–6.2, 6.5, and 6.8 km/s. A high-velocity (7.0–7.4 km/s) lower crust, which is common beneath platforms and shields [*Holbrook et al.*, 1992; *Rudnick and Fountain*, 1995; *Christensen and Mooney*, 1995], is not present. The seismic velocity beneath the Moho is a typical continental value of 8.0 ± 0.1 km/s. *Dong et al.* [1996] used a portion of these same seismic refraction data to get a preliminary crustal model that differs in several important details from our paper. For example, their model has no upper crustal high-velocity (6.3 km/s) zone beneath the UHP belt (Figure 7), and no Moho offset beneath the Xinyang-Shucheng fault (Figure 9). Our model contains more details than that of *Dong et al.* [1996] because we have modeled the complete data set with a combination of finite difference travel time and 2-D ray trace methods.

The structure of eastern China, including the Dabie Shan, is comparable to highly extended crust, which has an average thickness of 30.5 ± 5.3 km and average crustal velocity of 6.21 ± 0.22 km/s [*Li and Mooney*, 1998; *Christensen and Mooney*, 1995; *Rudnick and Fountain*, 1995]. Recent global seismic tomographic inversions indicate that the lithosphere is significantly thinner beneath eastern China than beneath the Siberian craton, Canadian shield, or Baltic shield [*Ekström et al.*, 1997]. These observations indicate that the lithosphere has been thinned in eastern China, including beneath the Dabie Shan, and that the crust has undergone moderate extension. This interpretation is supported by high heat flow (58–87 mW/m^2) and quantitative modeling that suggests a lithospheric thermal thickness of <100 km [*Yuan*, 1996]. Taking these observations further, *Gao et al.* [1998] and *Kern et al.* [1998] speculate that a mafic (eclogitic) lower crust in eastern China,

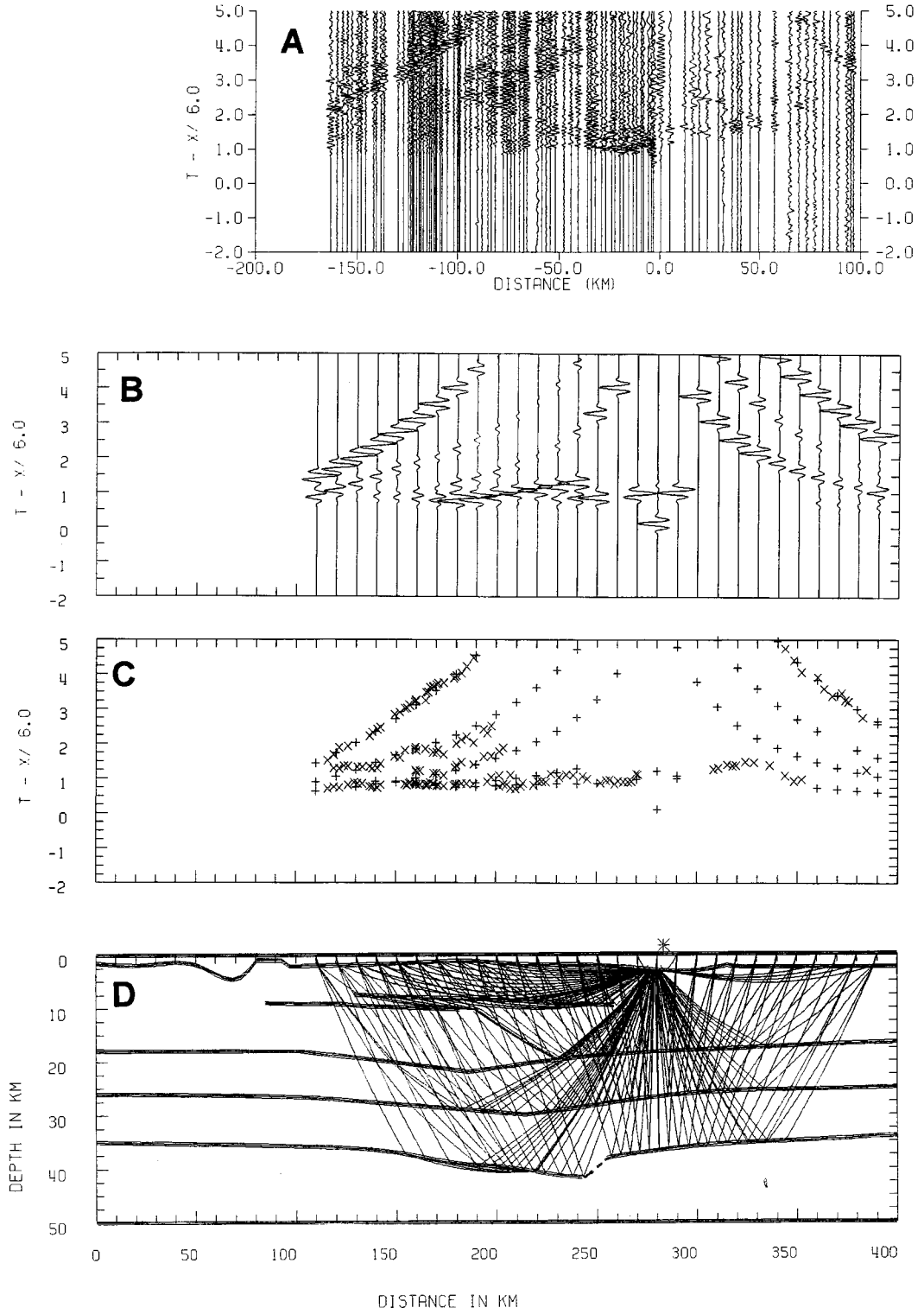

Figure 8. Calculation of ray tracing and 2-D synthetic seismogram and comparison with the observed data of shot point BuT. (a) Record section with normalized trace. (b) Trace-normalized synthetic record section. Amplitudes are generally stronger than observed data because seismic scattering and attenuation have been neglected. (c) Observed and calculated travel times, where crosses and pluses denote the observed and calculated travel times (s), respectively, with a reduced velocity of 6.0 km/s. (d) Ray paths, where asterisk denote shot point.

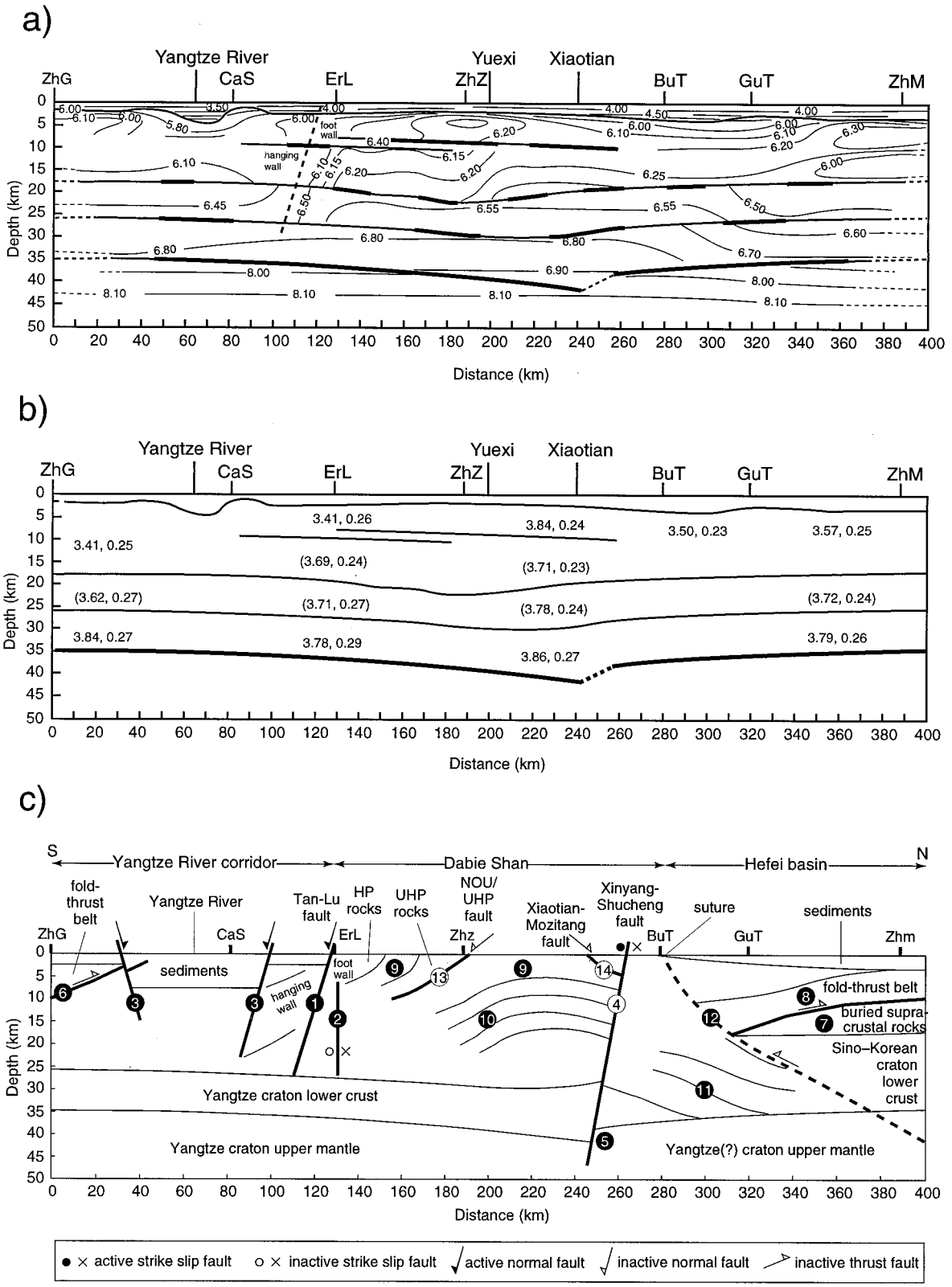

Figure 9. Final 2-D crustal model of the Dabie Shan. (a) *P* wave crustal structure. The velocity of upper crust (0–7 km) is determined from *Pg* using the finite difference inversion. The interfaces were determined by the arrival times of the wide-angle reflection and *Pn* waves from the all eight shots. Dashed line indicates the Moho offset. Velocities are accurate to better than 3%; depth of boundaries is accurate to better than 10% of the total depth [*Mooney*, 1989]. (b) *S* wave velocity and Poisson's ratio in the crustal structure, which has the same interfaces as the *P* wave model. Velocities and Poisson's ratios denoted with brackets indicate larger uncertainties (~5% in shear wave velocity; ~15% in Poisson's ratio). (c) Geological interpretation of Dabie Shan orogenic structure. See discussion, including key to numbers, in text.

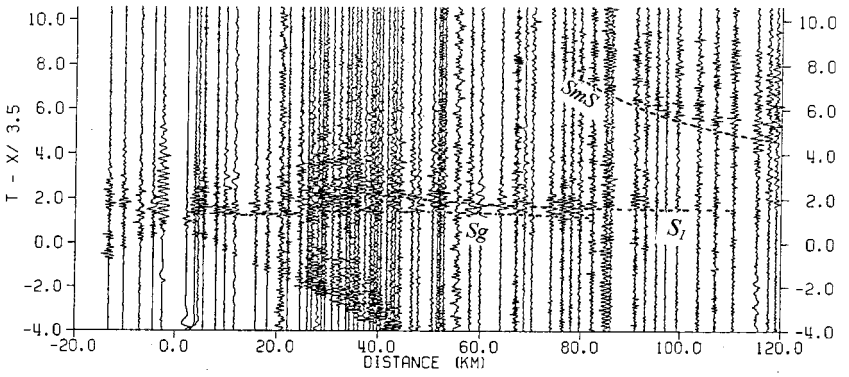

Figure 10. Record section with *S* wave arrivals (radial component), plotted with reduced velocity 3.50 km/s of shot point ErL. The direct arrival Sg, intracrustal reflection S_1, and Moho reflection SmS are clearly observed. Additional intracrustal reflections are generally weak and are variably recorded from other shot points. The quality of the *S* wave data in this record section is typical of the other shots recorded in this study.

including the Dabie Shan, was delaminated and recycled into the upper mantle during Cenozoic crustal extension.

We have combined our seismic model and the geological interpretation of *Hacker et al*. [1998] in a speculative crustal cross section of the Dabie Shan (Figure 9c). Referring to the numbered structural elements in Figure 9c, the active Tan-Lu fault (1) is an east dipping normal fault with a clear seismic signature defined by higher velocities in its footwall. As noted earlier, the conventional interpretation of the Tan-Lu fault is that it began as a Triassic sinistral strike-slip fault [e.g., *Yin and Nie*, 1993]; steep velocity gradients (2) east of the interpreted position of the modern Tan-Lu fault may reflect this older structure. Oblique normal faults that bound the Yangtze River SE of the Dabie Shan (3) can also be correlated with velocity gradients. An active sinistral strike-slip fault near the northern topographic limit of the Dabie Shan, the Xinyang-Shucheng fault (4), has no clear seismic signature within the crust; however, we speculate that it is responsible for the observed Moho offset (5). The seismic velocity structure south of the Dabie Shan may reflect contractional deformation associated with the fold-thrust belt (6). Likewise, we interpret the seismic velocity structure beneath the northern Hefei basin as reflecting thrusting in the hanging wall of the Sino-Korean crust, with middle crustal rocks (8) over supracrustal rocks (7). More speculatively, we tie the homoclinal south dipping foliation and south plunging lineation within the high- to ultrahigh-pressure section exposed in the southern Dabie Shan [*Hacker et al*., 1995b] to the northward increasing velocity gradient at (9). *Hacker et al*. [1998] described the pre-Cretaceous structure of the Dabie Shan as a crustal-scale antiform formed by warping of the high- to ultrahigh-pressure slab drawn southward out from beneath the Sino-Korean craton. We postulate that northward increasing velocity gradients at (10) and southward increasing velocity gradients at (11) are part of this antiform, which uplifts rocks with midcrustal velocities into the upper crust. This leads further to the implication that the suture between the two cratons is north of this antiform (not at the Moho offset), and we speculatively show it at location (12), dipping north beneath the trace of the isotopically defined crustal suture [*Hacker et al*., 1998]. Cretaceous normal faults that bound the southern (13) and northern (14) edges of the northern Dabie Shan magmatic-extensional complex have no clear seismic signature.

9. Conclusions

The crustal structure of the Dabie Shan has been determined from a new deep seismic refraction profile. In the shallow crust beneath the exposed ultrahigh pressure (UHP) rocks, there is a broad (50 km wide) high-velocity (6.2–6.3 km/s) zone centered at a depth of 4–5 km and a thin (1 km thick) high-velocity (6.4 km/s) layer at a depth of 8 km. Below 9 km, the middle and lower crust beneath the UHP zone are very similar to the crust to the north and south (i.e., beneath the Sino-Korean and Yangtze cratons, respectively). This suggests that UHP rocks are primarily concentrated in the upper crust (above 9 km depth) of the orogen. Our seismic model indicates that ecolgite is not volumetrically significant within the middle or lower crust.

There is only a modest (6.5 km deep) crustal root beneath the Dabie Shan. The thickness of the crust ranges from ~35 km beneath the Yangtze and Sino-Korean cratons to a maximum of 41.5 km at the northern margin of the Dabie Shan. The small variation in depth to the Moho along this 400-km-long profile indicates that the crust involved in the Triassic collision has undergone postcollisional thinning. This has been accomplished by a combination of isostatic uplift, erosion, and moderate crustal extension. An observed Moho offset is likely due to an active strike-slip fault. Much of the Triassic structure associated with the formation of the orogen and UHP rocks has been obscured by post-Triassic events. However, the crustal velocity structure determined for this profile is compatible with a north dipping suture located north of the Dabie Shan (Figure 9c) and an antiformal culmination of UHP rocks in the center of the Dabie Shan (Figure 7).

Acknowledgments. This research was jointly supported by the Natural Sciences Foundation of China and the Chinese Joint Earthquake Sciences Foundation under grants NSFC49374208 and JESF94-031. The fieldwork was conducted with the assistance of X. K. Zhang, B. Y. Chen, X. B. Chen, and the Geophysical Prospecting Center of the China Seismological Bureau. The authors wish to express their sincere thanks to those who helped. Copies of these data may be requested from the first author. We thank J. A. Hole for providing the finite difference travel time inversion code used in this study. R. C. Coleman, K. Favret, R. W. Girdler, and R. Meissner provided constructive comments on a early version of this paper. Reviews by A. R. Levander, D. M. Fountain, and an anonymous reviewer led to significant revi-

sions of the submitted manuscript. The authors are grateful to all of these reviewers. The first two authors were supported by the USA-PRC Protocol Agreement for Scientific and Technical Cooperation in Earthquake Studies as visiting scholars at the U.S. Geologic Survey in Menlo Park, California. B. R. Hacker was supported by NSF grants EAR-9417958 and EAR-9796119.

References

Ammon, C. J., and J. E. Vidale, Tomography without rays, *Bull. Seismol. Soc. Am*., *83*, 509–528, 1993.

Catchings, R. C., and W. D. Mooney, Basin and Range crustal and upper mantle structure along the 40°N parallel, northwest Nevada, *J. Geophys. Res*., *96*, 6247–6267, 1991.

Cerveny, V., and I. Psencik, SEIS83-numerical modeling of seismic wavefield in 2-D laterally varying layered structures by the ray method, in *Documentation of Earthquake Algorithms*, edited by E. R. Engdahl, *Rep. SE-35*, pp. 36–40, World Data Center (A) for Solid Earth Geophysics, Boulder, Colo., 1984.

Cerveny, V., I. A. Molotkov, and I. Psencik, I, *Ray Method in Seismology*, Univerzita Karlova, Prague, 1977.

Chen, W. J., Q. Li, D. Li, X. Wang, Geochronological implications of K/Ar isotope system of fault gouge—a preliminary study, *Phys. Chem. Earth's Inter.*, *17*, 17–23, 1988.

Christensen, N. I., Poisson's ratio and crustal seismology, *J. Geophys. Res*., *101*, 3139–3156, 1996.

Christensen, N. I., and W. D. Mooney, Seismic structure and composition of the continental crust: A global review, *J. Geophys. Res*., *100*, 9761–9788, 1995.

Dong, S., X. Wu, R. Gao, D. Lu, Y. Li, Y. He, J. Tang, F. Gao, M. Hou, and D. Huang, Preliminary study on deep geology of Dabie orogenic belt, in *Continental Dynamics*, vol. 1, pp. 103–108, Chin. Acad. of Geol. Sci., Beijing, 1996.

Ekström, G., J. Tromp, and E. W. Larson, Measurements and global models of surface wave propagation, *J. Geophys. Res*., *102*, 8137–8158, 1997.

Gao, S., B. R. Zhang, Z. M. Jin, H. Kern, Z. D. Zhao, T. C. Luo, How mafic is the lower continental crust?, *Earth Planet. Sci. Lett.*, *161*, 101–117, 1998.

Group of Industrial Explosion Observation, Differences of the crustal structures among the areas of Henan, Hubei and Shaanxi provinces (in Chinese), in *Progresses on the research of Deep Structure in Chinese Continent*, pp. 192–204, Geol. Publ. House, Beijing, 1988.

Hacker, B. R., and Q. C. Wang, Ar/Ar geochronology of ultrahigh-pressure metamorphism in central China, *Tectonics*, *14*, 994–1006, 1995.

Hacker, B. R., L. Ratschbacher, L. Webb, and S. Dong, What brought them up? Exhumation of the Dabie Shan ultrahigh-pressure rocks, *Geology*, *23*, 743–746, 1995a.

Hacker, B. R., X. Wang, E. A. Eide, and L. Ratschbacher, Qinling-Dabie ultrahigh-pressure collisional orogen, in *Tectonic Evolution of Asia*, edited by A. Yin and T. M. Harrison, Cambridge Univ. Press, 1995b.

Hacker, B. R., L. Ratschbacher, L. Webb, T. Ireland, D. Walker, and S. Dong, U/Pb zircon ages constrain the architecture of the ultrahigh-pressure Qinling-Dabie Orogen, China, *Earth Planet. Sci. Lett.*, *161*, 215–230, 1998.

Holbrook, W. S., W. D. Mooney, and N. I. Christensen, The seismic velocity of the deep continental crust, in *Continental Lower Crust*, edited by D. M. Fountain, R. Arculus, and R. W. Kay, pp. 1–34, Elsevier, New York, 1992.

Hole, J., Nonlinear high-resolution three-dimensional seismic travel time tomography, *J. Geophy. Res*., *97*, 6553–6562, 1992.

Hu, H. X., X. B. Chen, and B. X. Zhang, Interpretation of deep seismic sounding data from the Suixian-Anyang profile in central China (in Chinese), *Acta Seismol. Sin.*, *8*, 37–49, 1986.

Jarchow, C., G. A. Thompson, R. Catchings, and W. D. Mooney, Seismic detection of active magmatic underplating beneath the Basin and Range Province, western United States, *J. Geophys. Res*., *98*, 22,095–22,108, 1993.

Kern, H., S. Gao, Z. M. Jin, T. Pill, and S. Y. Jin, Petrophysical studies on rocks from the Dabie ultrahigh-pressure (UHP) metamorphic belt, Central China: implications for the composition and delamination of the lower crust, *Tectonophysics*, in press, 1998.

Levander, A. R., and K. Holliger, Small scale heterogeneity and large-scale velocity structure of the continental crust, *J. Geophys. Res*., *97*, 8797–8804, 1992.

Levander, A., R. W. England, S. K. Smith, R. W. Hobbs, J. A. Goff, and K. Holliger, Stocastic characterization and the seismic response of upper and middle crustal rocks based on the Lewisian gneiss complex, Scotland, *Geophys. J. Int*., *119*, 243–259, 1994.

Li, S., and W. D. Mooney, Crustal structure of China from deep seismic sounding profiles, *Tectonophysics*, *288*, 105–113, 1998.

Liou, J. G., X. Wang, R. G. Coleman, Z. M. Zhang, and S. Maruyama, Blueschists in major suture zones of China tectonics, *Tectonics*, *8*, 609–619, 1989.

Liou, J. G., R. Y. Zhang, E. A. Eide, S. Maruyama, X. Wang, and W. G. Ernst, Metamorphism and tectonics of high-P and ultrahigh-P belts in Dabie-Sulu Regions, eastern central China, in *Tectonic Evolution of Asia*, edited by A. Yin and T. M. Harrison, Cambridge Univ. Press, New York, 1995.

Luetgert, J. H., MacRay: Interactive two-dimensional seismic raytracing for the Macintosh, *U.S. Geol. Surv. Open File Rep., 92-356*, 1992.

Meissner, R., *The Continental Crust: A Geophysical Approach*, 426 pp., Academic, San Diego, Calif., 1986.

Mereu, R. F., and S. B. Ojo, The scattering of seismic waves through a crust and upper mantle with random lateral and vertical velocity inhomogeneities: *Phys. Earth Planet. Inter.*, *26*, 233–240, 1981.

Mooney, W. D., Seismic methods for determining earthquake source parameters and lithospheric structure, in *Geophysical Framework of the Continental United States*, edited by L. C. Pakiser and W. D. Mooney, *Mem. Geol. Soc. Am*., *172*, 11–34, 1989.

Mooney, W. D., and T. M. Brocher, 1987, Coincident seismic reflection/refraction studies of the continental lithosphere: A global review, *Rev. Geophys*., *25*, 723–742.

Ojo, S. B., and R. F. Mereu, The effect of random velocity fluctuations on the travel times and amplitudes of seismic waves, *R. Astron. Soc. Geophys. J.*, *84*, 607–618, 1986.

Qiu, G. H., and Q. B. Guo, 1:500,000 gravity anomaly mapping of the Dabie shan area in Hubei, Henan, and Anhui provinces and discussion on the tectonics (in Chinese), *Anhui Geosci. Technol.*, *2*, 53–66, 1989.

Rudnick, R. L., and D. M. Fountain, Nature and composition of the continental crust: A lower crustal perspective, *Rev. Geophys*., *33*, 267–309, 1995.

Vidale, J. E., Finite-difference calculation of travel-times, *Bull. Seismol. Soc. Am*., *78*, 2062–2076, 1988.

Vidale, J. E., Finite-difference calculation of travel-times in three dimensions, *Geophysics*, *55*, 521–526, 1990.

Wang, C. Y., Z. Y. Lin, and X. B. Chen, Comprehensive study of geophysical data on geoscience transect from Menyuan, Qinghai Province, to Ningde, Fujian Province, China, *Acta Geophys. Sin.*, *39*, 590–598, 1995.

Xu, J. W., G. Zhu, W. X. Tong, X. R. Cui, and Q. Liu, Formation and evolution of the Tancheng-Lujiang wrench fault system: a major shear system to the northwest of the Pacific Ocean, *Tectonophysics*, *134*, 273–310, 1987.

Ye, S., J. Ansorge, E. Kissling, and St. Mueller, Crustal structure beneath the eastern Swiss Alps derived from seismic refraction data, *Tectonophysics*, *242*, 199–221, 1995.

Yin, A. and S. Nie, An indentation model for the North and South China collision and the development of the Tanlu and Honam fault systems, eastern Asia, *Tectonics*, *12*, 801–813, 1993.

Yuan, X. C., *Atlas of Geophysics of China*, 216 pp., Geol. Publ. House, Beijing, 1996.

Yuan, X. C., M. C. Xu, W. B. Tang, and Q. H. Wang, Seismic reflection profile on eastern Qinling continental crust (in Chinese), *Acta Geophys. Sin.*, *37*, 749–758, 1994.

Zeng, R., W. Sun, T. Mao, Z. Lin, H. Hu, and G. Chen, The map for the depth of Moho discontinuity in Chinese continent, *Acta Seismol. Sin.*, *17*, 322–327, 1995.

Zheng, Y., and J. W. Teng, Crustal and upper mantle's structure in Suixian-Ma'an Shan area and some characteristics on the Tan-Lu tectonic zone (in Chinese), *Acta Geophys. Sin.*, *32*, 648–652, 1989.

B. R. Hacker, Geological Sciences, University of California, Santa Barbara, CA 93160-9630.

W. D. Mooney, U.S. Geological Survey, MS 977, 345 Middlefield Road, Menlo Park, CA 94025. (mooney@usgs.gov)

C.-Y. Wang and R.-S. Zeng, Institute of Geophysics, State Seismological Bureau, Beijing, 100081, China.

(Received June 9, 1998; revised November 3, 1999;
accepted November 15, 1999.)